Continuous additive manufacturing of hemp yarn-reinforced biocomposites with improved impregnation method

Geoffrey Ginoux, Xikun Wu, Chaimae Laqraa, Damien Soulat, Joseph Paux, Manuela Ferreira, Ahmad Rashed Labanieh, Samir Allaoui

Continuous additive manufacturing of hemp yarn-reinforced biocomposites with improved impregnation method

GEOFFREY GINOUX[1,*], XIKUN WU[1], CHAIMAE LAQRAA[2], DAMIEN SOULAT[2], JOSEPH PAUX[1], MANUELA FERREIRA[2], AHMAD-RASHED LABANIEH[2], SAMIR ALLAOUI[1]

[1]*University of Reims Champagne-Ardenne, Institut de Thermique, Mécanique, Matériaux (EA 7548), MATUR Chair – Campus Sup Ardenne, 08000 Charleville-Mézières (France)*

[2]*University of Lille, ENSAIT – Laboratoire de Génie et Matériaux Textiles (GEMTEX), 59056 Roubaix (France)*

**Email: geoffrey.ginoux@univ-reims.fr*

Abstract.

This study was motivated by the development of new additively manufactured bio-based materials with high performance. Hemp yarn was used in continuous material extrusion additive manufacturing to produce novel hemp yarn-reinforced biocomposites. The hemp yarn was compared to an original hemp/poly(lactic acid) hybrid yarn prepared by commingling before printing as an improved impregnation method. In X-ray micro-computed tomography, the hybrid yarn-based biocomposite exhibited a higher impregnation rate accompanied by a reduced void content, more aligned fibers, and a more homogeneous distribution of the different constituents, resulting in significantly higher mechanical properties during tensile loading with a more brittle behavior compared to the additively manufactured biocomposite based on pure hemp yarn. In addition, superior mechanical performance was obtained while having lower fiber fraction with the use of hybrid yarns, raising awareness about the importance of improving the impregnation of the plant fibers as well as the fiber volume fraction. This original preparation method can provide bio-based materials with enhanced quality and performance, close to those obtained with conventional manufacturing techniques, while making the most of additive manufacturing for sustainable, lightweight, and high-end applications in health or aerospace.

Keywords: A. Polymer-matrix composites (PMCs), A. Natural fiber composites, B. Mechanical properties, D. X-ray micro-computed tomography, E. Additive manufacturing

1. Introduction

Since the late 1980s, layer-by-layer additive manufacturing (AM), also known as “3D printing”, has been developing from rapid prototyping to production of end-use products with benefits such as design freedom, faster fabrication line, and lower cost for complex parts or small productions [1]. One of the most widespread AM techniques is material extrusion additive manufacturing (MEAM), thanks to its ease of use and cost-effectiveness [2]. Polymer-based MEAM technologies

essentially include fused filament fabrication (FFF) and, since the last decade, FFF-derived technologies based on in-nozzle impregnation that manufacture composites by combining a molten polymer with a continuous reinforcement through a nozzle [3]. With the development of AM for technical and high-end applications, such as general industry, healthcare, automotive, or aerospace, the specifications demand materials with high performances – including but not limited to the mechanical properties – that are difficult to attain with current additively manufactured materials [4]. Moreover, AM of composites is a way to functionalize and improve the performances of a polymer-based material [5,6]. First attempts were accomplished with micro- and nano-filled composites by FFF [7,8]. Still, the performance only tends to get closer to the requirements of high-end applications with the AM of continuous-reinforced composites whose mechanical properties can be similar to those of conventional composites [9].

The main limitations of continuous-reinforced composites by AM concern the lack of materials availability and achievable properties with new functionalities, which prevents the technology from being developed for a broader range of applications [8,10,11]. Most of the commercial continuous-reinforced composite filaments are synthetic pre-impregnated carbon, glass, basalt, and aramid fibers, which are those primarily studied in the literature [9,12–14]. More recently, with the need to develop more environment-friendly materials, plant fibers-based materials have been developing in AM, especially with bio-sourced matrices [15,16]. Their properties are already well-known in conventional composites and present advantages compared to synthetic fibers-based composites, including high damping properties [17], acoustic insulation [18], and other general advantages – namely low cost, low density, low hazard, and so on – in automotive and civil engineering [19]. A plethora of plant fibers are used in AM, but mainly as short fibers, while long plant fibers are more focused on flax yarns and, to a lesser extent, on yarns based on ramie, jute, or pineapple leaf fibers [20] that can be adapted to large structural parts for high-end applications [21]. Despite the absence of studies on continuous hemp reinforcements in AM, hemp fibers have mechanical properties similar to or just lower than those of flax fibers [22,23]. Hemp also presents economic and ecological advantages during its easy growth, such as little or no herbicide, fungicide, pesticide, and fertilizer due to its vigorous nature compared to other plants [24,25]. Like flax, hemp cultivation improves the quality of soil by carbon sequestration [26] and heavy metal extraction [27], making hemp an interesting candidate as an alternative and environmentally friendly reinforcement for yarn-reinforced composites (YRC) by AM. However, hemp fibers have a high variability [28,29], that explains the range of mechanical properties [29,30], which is accentuated by technological barriers from the transformation process that cause its lower maturity [31] and lead the current efforts to improve hemp fibers' processability and properties compared to flax fibers [29,32].

Whatever the plant source, continuous reinforcements based on plant fibers in AM suffer from poor impregnation quality because of the chemical composition and structure of natural fibers and their associated yarns, which are different from the

smooth and untwisted synthetic ones [3,23,33]. Yet, this impregnation is needed to develop optimal stress transfer from the polymeric matrix to the fibers and obtain maximum mechanical properties for the composites [34]. The literature agrees on the lack of pressure and the short process time that prevent the impregnation of the fibers by the highly viscous molten polymer [10,35]. Several studies intend to improve the quality of the additively manufactured YRC by chemical compatibilization treatments [36], by parametric optimization of the printing process [37,38], or by composite filament preparation prior to printing thanks to a pre-impregnation [39,40]. None of these studies fully succeeded in impregnating the plant fibers-based yarns in printed composites as void contents are reduced but still observed. In another way, recent studies performed commingling before AM with the use of synthetic materials, namely commingled yarns based on continuous E-glass fibers and polypropylene fibers [41] and ones based on continuous carbon fibers and polyamide 6 fibers [42]. These studies demonstrate the viability of such commingling preparation upstream of AM to have a more intimate mixing and to fully impregnate the fibers during AM, which develops maximum fiber/matrix interface. In the same way, commingling can be a promising preparation technique of plant fibers-based yarns for AM. Still, the previous researches [41,42] were performed with continuous synthetic fibers that are easier to impregnate as their surface is smoother than that of plant fibers and as the yarns are untwisted [33]. Such preparation could be adapted from the plant hybrid yarns already used in conventional composite manufacturing [43].

To the authors' knowledge, both long hemp fibers and commingled yarns based on plant/thermoplastic fibers have never been attempted in continuous AM. A novel preparation method of yarns is then proposed in this study for the continuous AM of YRC by commingling plant fibers and bio-sourced polymer fibers, namely hemp fibers and poly(lactic acid) (PLA) fibers. Two original hemp yarn-reinforced biocomposites (HYRB) were manufactured (i) from hemp yarns and (ii) from hemp/PLA commingled hybrid yarns for comparison of their printability, their induced structures and morphologies, and their developed mechanical properties, regarding commingling prior to AM. Characterization techniques were carried out on both HYRB materials via X-ray micro-computed tomography (X-µCT), digital 3D microscopy, and tensile tests to evaluate the materials-process-structure-properties relationships. A chemical extraction method is also proposed to precisely determine the fiber mass fractions in the HYRB materials with the aim of better assessing the mechanical behavior related to the composite formulation.

2. Materials and methods

2.1. Preparation of the yarns

Low-twisted and untreated hemp yarns were provided by the Italian Company Linificio e Canapificio Nazionale. They were produced from hackled and combed hemp fibers. Their textile – namely linear density and twist level – and

mechanical properties – namely tenacity and elongation at break – are given in Table 1 and were identified in previous studies dedicated to the weaveability of these yarns to optimize composite properties made from these raw materials [44–46]. These yarns are denoted as the "H0" yarns.

Table 1. Main properties of the H0 hemp yarns.

Properties	Values
Linear density	316 ± 4 tex
Twist level	39 ± 2 tpm
Tenacity	9.31 ± 1.42 cN/tex
Elongation at break	1.82 ± 0.08%

These H0 pure-hemp yarns were also used to be mixed with PLA fibers to produce commingled yarns, namely hemp/PLA hybrid yarns. This manufacturing process allows a good combination of natural and thermoplastic fibers at the microscale. Previous studies of these hemp blends with PA12 or PA11, developed on a roving scale, have demonstrated the weaveability of these commingled yarns and have focused on the mechanical properties of composite samples obtained by thermocompression of these stacked reinforcements [47,48]. However, to the authors' knowledge, no studies have been carried out on the use of these plant-based commingled yarns to produce composites by AM. In this study, with the aim of improving the core mixing between hemp and thermoplastic fibers, the manufacturing process of these commingled yarns was in two stages. First, an intimate blend between the hemp fibers and the PLA fibers was produced on a draw frame (Gills). Three hemp slivers and three PLA slivers were introduced in this machine and were then drawn to obtain a single hybrid sliver. A second pass on Gills was carried out to obtain a homogeneous hemp/PLA sliver. In a second step, this sliver was drawn and wrapped with a 100 dtex PLA multifilament on a hollow spindle machine to obtain a hemp/PLA commingled hybrid yarn. The main properties of these yarns are given in Table 2 and are denoted as "HybHP" yarns hereafter.

Table 2. Mains properties of the HybHP hemp/PLA commingled yarns.

Properties	Values
Linear density	557 ± 16 tex
Twist level	200 tpm
Hemp volume fraction	39%

At this stage, these raw materials for the AM, as H0 yarns (Table 1) and HybHP yarns (Table 2), are used in a dry state, with no prepreg stages, which renders flexible materials with no intermediate thermal pre-processing prior to AM, in opposition to other studies [39]. This preparation of the yarns is thought to prevent any thermal degradation of the materials while being energy-cost saving.

2.2. Preparation of the specimens

HYRB-based materials were printed using a Composer A4 printer from Anisoprint (Luxembourg). Its printhead consists of two material extrusion elements. The first one is an FFF-based element that allows the printing of pure thermoplastic materials through a nozzle of 0.4 mm in diameter (see left part in Figure 1). The second one is a Continuous Fiber Coextrusion (CFC)-based element that coextrudes a thermoplastic filament and a composite filament, made of continuous pre-impregnated fibers, and deposits a continuous-reinforced composite through a nozzle of 0.8 mm in diameter. In this study, the composite filament is replaced by a yarn, while the thermoplastic filament remains to continuously coat the yarn, both for the H0 and HybHP yarns. The CFC-based element was modified to be adapted to the yarn-based materials' specifications, with the yarn being pulled by the cooled YRC deposition rather than pushed by a feeding system prior to the heating elements (in red in Figure 1). The CFC-based element is now renamed as the Continuous Yarn Coating (CYC)-based element to be more accurate and better reflect the developed apparatus (see right part in Figure 1).

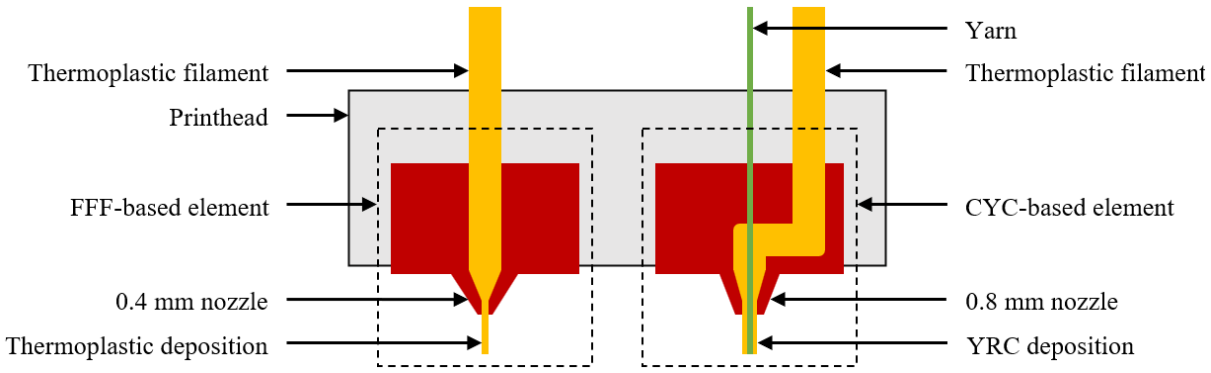

Figure 1. Schematic representation of the multi-materials extrusion AM process based on FFF and CYC technologies.

Thermoplastic materials for the FFF and CYC-based elements were PLA filaments under the reference PLA EF 3D850 in their native colors and were supplied by Nanovia (France). The physical properties of the PLA filaments are displayed in Table 3, as provided by the supplier. The yarns for the CYC-based element were either the H0 yarn or the HybHP yarn described above. Each yarn was used independently to prepare H0 and HybHP materials by AM, respectively. All filaments and yarns were dried at 50 °C in a ventilated oven for 12 h before printing.

Table 3. Physical properties of PLA EF 3D580 filament as supplied by Nanovia.

Properties	Values
Diameter	1.75 mm
Density	1.24 g/cm^3
Glass temperature	55-60 °C
Melt Flow Rate	7-9 g/10 min
Young's modulus	3540 MPa
Ultimate tensile strength	58 MPa
Elongation at maximum strength	2.6%
Izod impact	1.18 kJ/m²

Specimens for microstructural and mechanical characterizations were prepared by machining them into printed plates to ensure homogeneity in the induced microstructures and representativeness of the specimens regarding scale effect and mechanical properties [49]. Plate geometry and dimensions are detailed in Figure 2(a) as designed for slicing of the STL file. The stacking sequence of the biocomposites was set in Aura slicer software from Anisoprint. It consisted of a first layer of PLA of 0.1 mm in height to allow adhesion of the part on the build plate, followed by five layers of 0.4 mm in height each. These five layers consisted of three HYRB layers as fiber-reinforced plies between two PLA layers for cohesion and surface quality improvement (see Figure 2(b)). Other printing parameters were also set in Aura software (see Table 4) to generate a GCODE file readable by the Composer A4 printer. After printing the two HYRB-based plates, one with the H0 yarn, and the other with the HybHP yarn, five specimens were cut from each plate with a TS 55 FEBQ rotative steel plate saw from Festool (Germany) along the x-axis to manufacture 0°-oriented specimens (see Figure 2(a)).

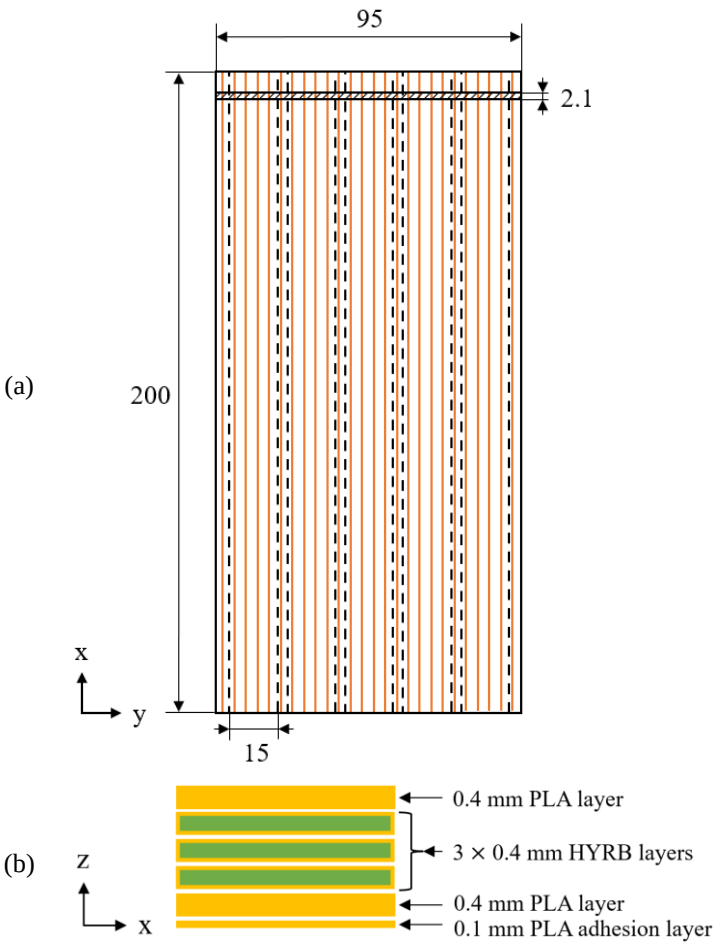

Figure 2. HYRB-based printed plate design for machining a set of five specimens with (a) plate geometry and dimensions expressed in millimeters and (b) stacking sequence of the biocomposite. Orange lines represent the deposition orientation along the length of the plate. Dashed lines represent the machining paths after plate printing.

Table 4. General printing parameters and associated values for the continuous AM of HYRB-based plates.

Parameters	Values
FFF printing speed	40 mm/s
CYC printing speed	15 mm/s
FFF extruder temperature	230 °C
CYC extruder temperature	230 °C
Build plate temperature	60 °C
Envelope temperature	32 °C
FFF raster width	0.40 mm
CYC raster width	0.80 mm
Infill orientation (x-axis)	0°
Fill density	100%
Number of perimeter contours	0

2.3. Characterization and extraction

Microstructures in the middle and at the end of H0 and HybHP specimens were observed thanks to a Desk-Tom 150 X-µCT from RX Solutions (France) to assess the print quality of the HYRB-based specimens in the gauge section and at the specimen's end where the trajectory performed a 180°-turn, denoted as a "U-turn". The X-ray source was set to 60 kV in voltage and 166 µA in current intensity, and X-rays were detected with a 1920 × 1536 pixels scintillation detector. 1440 radiographic images were captured at 1.6 images/s with a voxel size of 10.0 µm to acquire the entire width and height of the effective cross-sectional area of the specimens. The same was applied to partial specimens obtained from smaller cut samples to acquire microstructure with a higher resolution of 4.4 µm in voxel size regarding the impregnation quality of the yarns by the PLA matrix in both HYRB-based specimens. Based on these 2D images, 3D volume reconstructions were carried out on X-Act software from RX Solutions, and VGL files were generated. 4.0 × 2.6 × 2.2 mm^3 (XYZ) volumes were selected on 3D images with a voxel size of 4.4 µm to frame 3 × 3 rasters over a 4.0 mm deposition length (see brown dotted frame in Figure 3) for in-HYRB porosity rate measurements using the porosity analyzer module of VGStudio MAX software from Volume Graphics (Germany). 4.0 × 0.7 × 0.3 mm^3 (XYZ) volumes were also selected on 3D images with a voxel size of 4.4 µm inside one yarn for in-yarn porosity rate measurements (see red dotted frame in Figure 3). For both kinds of porosity rates and both HYRB-based specimens, three different sampling zones were measured in porosity rate for statistical analysis. One should note that porosity measurements were not performed on the flexible yarns in input of continuous AM as tensile, torsion, and flexion strains at low stress can easily and locally affect the void size, which would make difficult the comparison in porosity rate between input materials and printed materials for the study. However, for the commercial PLA filaments, no porosity was observed by X-µCT analysis.

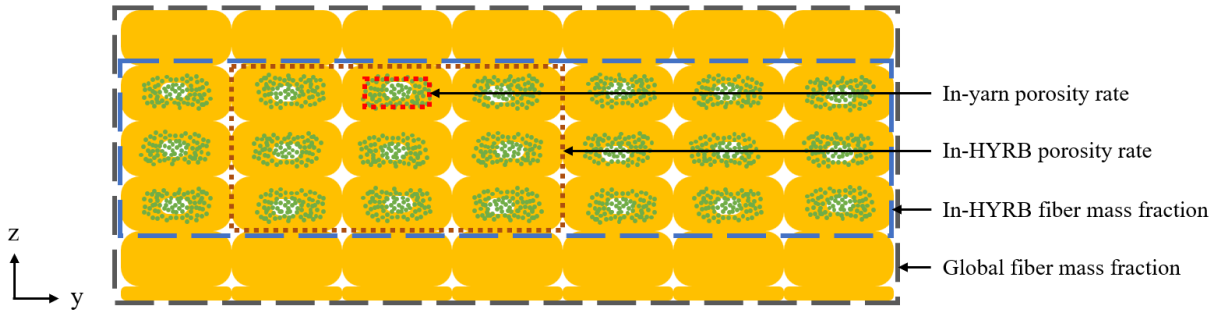

Figure 3. Schematic representation of the composition of the HYRB-based printed plates as seen through a cut orthogonal to the deposition direction. PLA matrix, hemp fibers, and voids are respectively shown in yellow, green, and white colors. Dotted lines represent examples of sampling for porosity rate measurements as determined by the X-µCT method and dashed lines for fiber mass fraction determination by the chemical extraction method.

As the densities between PLA and hemp are close, and the maximum resolution is of greater magnitude order than the hemp/PLA interfaces, the distinction between PLA and hemp was not achievable with the X-μCT method. Thermogravimetric analysis (TGA) is another common method to determine the mass fractions for the different constituents of a composite, but cellulose and PLA thermally degrade at the same temperature range around 300 to 360 °C [50]. Consequently, determining the mass fraction is strenuous in TGA with plant fibers/PLA composites, including hemp/PLA composites [51]. Instead, most studies on continuous additively manufactured YRC determined the fiber volume fraction thanks to process-related data or image analysis [3,34,52–55]. On the one hand, process input data allow the determination of a global fiber volume fraction, while the distribution of the fibers can be heterogeneous, either with the stacking sequence or with the fiber impoverishment in the U-turn zone [56]. On the other hand, determining the fiber volume fraction thanks to 2D images can be non-representative of a volume.

To relate the actual composite formulation in the specimens' effective section with the measured mechanical properties, a solvent extraction method is proposed to determine the fiber mass fractions (i) for the whole specimens and (ii) for the HYRB-only sections (see respectively gray dashed frame and blue dashed frame in Figure 3). For this purpose, and for both H0 and HybHP specimens, about 1.5 g were cut in the gauge section, dried in a ventilated oven at 40 °C for 12 h, and precisely weighted on an AE240 analytical balance from Mettler Toledo (Switzerland) with a precision of ± 0.01 mg before separating PLA layers from the HYRB layers. PLA and HYRB samples were then separately weighted with the same AE240 analytical balance. Each HYRB sample was then soaked for 48 h in 20 mL of analytical grade trichloromethane (99.8% $CHCl_3$) from VWR International (USA) at room temperature for solubilization of PLA before being filtrated by vacuum filtration through a Büchner funnel and rinsed with 25 mL of $CHCl_3$ three times. Soaking, filtration, and rinsing steps were repeated a second time before drying in a ventilated oven at 40 °C for 24 h. Dried fibers were finally weighted on the AE240 analytical balance for each prepared sample. The chemical extraction procedure was repeated three times on both H0 and HybHP specimens for statistical analysis.

The mechanical properties were measured on an Instron 3366 universal testing machine from Instron (USA) equipped with a 10 kN load cell and a video extensometer. Tensile tests were performed at a 2 mm/min crosshead speed at ambient conditions, namely 22 °C in temperature and 47% in humidity rate. The video extensometer recorded the strains of the specimens between two dark markers 50 mm apart and centered in the middle of the 140 mm gauge length (see Figure 4). All specimens were measured three times in thickness and width with an electronic caliper of ± 0.01 mm precision to calculate the cross-sectional area of each specimen. At least five specimens were tested for each configuration of HYRB-based material for statistical analysis. Dixon tests were conducted to verify the absence of abnormal values.

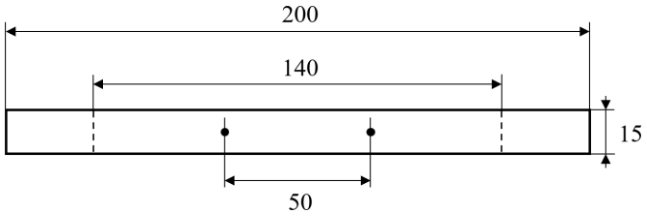

Figure 4. Tensile specimen design from ASTM D3039 with adapted dimensions, expressed in millimeters.

After testing, the facies of rupture were observed under a VHX-7000 4K digital 3D microscope from Keyence (Japan) equipped with a VHX-7100 fully integrated head and a VHX-E20 objective of ×20 to ×100 magnification range. All observations were recorded on 2880 × 2160 pixels images with ×80 magnification under reflected light. Several images were combined into one image to acquire a full-length fracture.

3. Results and discussion

3.1. Print quality

X-µCT analyses were first performed on the specimens' ends to observe the morphology of the HYRB layers at the U-turns. Figure 5 depicts representative U-turns in the HYRB layer of H0 and HybHP specimens. The denser the material is, the brighter it appears on tomographies, with fibers being the brightest, voids being the darkest, and polymer having an intermediate gray. Because of an ironing effect [56] and because the yarn is rather pultruded than extruded (see 2.2. Preparation of the specimens), yarns tend to retract in the U-turn and do not deposit over the whole trajectory length, reducing the dimensional accuracy. The more pressure the nozzle applies on the fibers, the more pronounced the effect. When comparing the retraction of the yarns on an average of twenty U-turns for both HYRB-based specimens, the missing length of yarns is 4.5 ± 0.5 mm from the H0 specimens' edge and 3.9 ± 0.3 mm for HybHP specimens (see yellow dashed lines in Figure 5). The difference is slight but still statistically significant (p-value = 0.0003), with a tendency for HybHP specimens to be more consistent in the U-turn depositions and to have a lower retraction. This means that the pressure applied by the nozzle is reduced and more homogeneous with HybHP yarns. This can be attributed to the addition of PLA fibers in the core of HybHP yarns, regarding H0 yarns, which constitutes a viscous medium that facilitates the deformation of the yarn. In the HybHP specimens, PLA is added in the HYRB layers through the thermoplastic filament and the HybHP yarn that already contains it (see CYC-based element in Figure 1), which leads to an increased amount of PLA in the composite compared to the H0 specimens. This is also observed in the retraction zone. As hemp yarns leave an absence of materials after retraction, only PLA and voids are left. In the case of H0 specimens (see Figure 5(a)), the retraction zone essentially consists of voids with PLA not reaching the entire width of the edge. On the opposite, HybHP specimens present

fuller retraction zones thanks to the presence of more PLA that can eventually flow out of the edge when the nozzle chases away the molten polymer (see Figure 5(b)). Last but not least, a change in trajectory could lead to poor impregnation with the formation of voids [57], which is observed in some buckles of the yarns in H0 specimens with the presence of larger voids (see Figure 5(a)), but not with HybHP specimens (see Figure 5(b)). Consequently, while both specimens present retraction, dimensional accuracy is best achieved with the HybHP specimens due to less retraction and fuller ends.

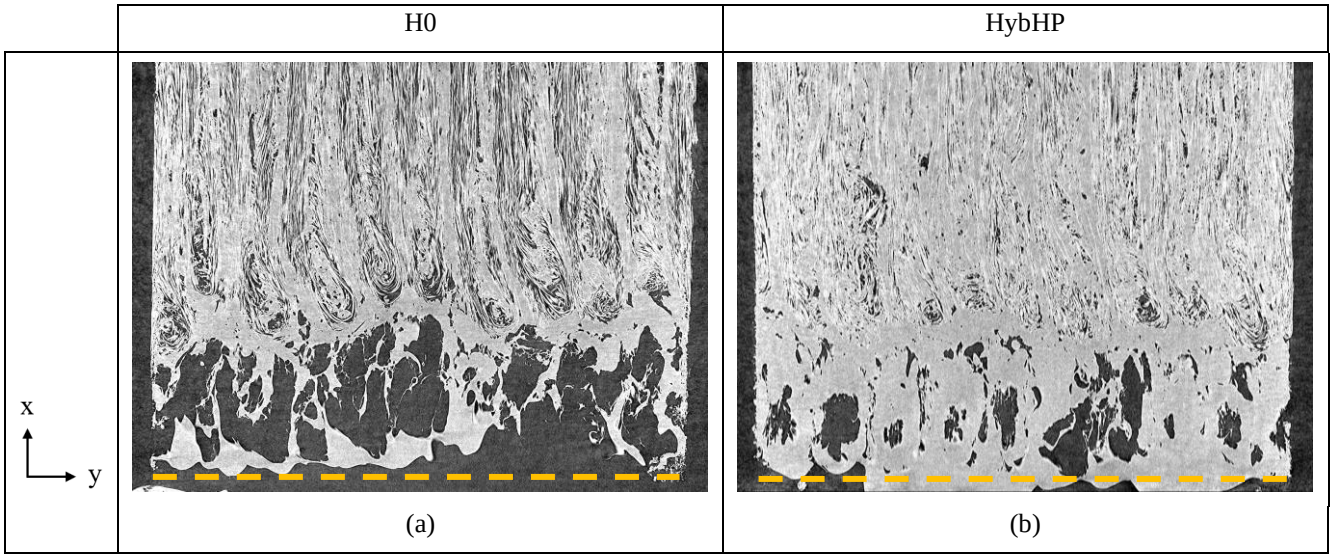

Figure 5. Tomographies of (a) H0 and (b) HybHP specimens at the U-turn as seen through an X-µCT cut in the plane of a HYRB layer. Yellow dashed lines represent the end of the specimens.

Looking at the surrounding of the U-turns towards the specimens' core, yarns in the H0 specimens are more visible and can be easily distinguished from one another, while those in HybHP are well distributed in the PLA matrix and are harder to differentiate from one yarn to another (see Figure 5). This difference is explained by two main reasons: changes in void morphology and diffusion of the fibers in the transverse direction due to lateral forces [58]. Firstly, for void morphology, H0 specimens present numerous voids with a high shape factor as the porosities are essentially longitudinal and oriented along the fibers in the deposition direction and inside the yarns (Figure 5(a)), which is attributed to a poor impregnation rate with inner dry fibers. On the contrary, HybHP specimens present fewer voids with a low shape factor as the porosities are more spherical (Figure 5(b)), which is attributed to a higher impregnation rate. The presence of round voids in the HybHP specimens can originate from the air entrapment that was between the hemp and PLA fibers in the HybHP yarns before printing. This means that commingling can reduce the void content between the plant fibers, but greater pressure is required to remove the residual air because of the more twisted and less deformable architecture compared to synthetic commingled yarns [33,41,42]. Secondly, fibers in the HybHP specimens (see Figure 5(b)) are well-distributed in the

transverse direction compared to fibers in H0 specimens (see Figure 5(a)) as the yarns in the H0 specimens are surrounded by polymer portions, while those in HybHP are side by side. This is explained by the pressure applied by the nozzle on the fibers and by the transverse flow of the polymer [58] that pushed the fibers away from the center of the raster during deposition. This enhanced transverse displacement of the deposited HybHP yarns can emanate from the lower hemp content in the HybHP yarns that offers less resistance to the polymer flow, by the greater PLA content that exerts more flow, and/or by a lubrication-like effect from the PLA matrix that reduces the friction between hemp fibers and then facilitates the displacement due to the improved impregnation quality.

X-μCT analyses were then performed on the mechanically untested gauge sections of the HYRB-based specimens to observe their morphology in the effective sections that can undergo mechanical stress. Figure 6 illustrates different and representative views of H0 and HybHP gauge sections. Like U-turns, H0 specimens mostly present longitudinal voids along the fibers (see Figure 6(a)), while HybHP specimens present fewer longitudinal voids in favor of rounder voids (see Figure 6(b)) because of the initial presence of PLA fibers in the HybHP yarns. Regardless of the void morphology, individual H0 yarns are less visible in the gauge section compared to the ones in the U-turns (see Figure 5(a)), meaning that, when getting away from the ends, the printing conditions, as well as the nature of the hemp fibers, are favorable to a spreading of the fibers in the transverse direction with respect to the deposition direction. Hemp fibers in H0 specimens are then distributed more homogeneously over the whole width of the specimen at a level comparable to the HybHP specimens (see Figure 6(a) and Figure 6(b)). However, fibers in H0 and HybHP specimens describe different morphologies regarding orientation with HybHP fibers mostly aligned in the deposition direction, i.e. unidirectionally oriented at 0°, whereas H0 fibers are oriented at various angles from 0° up to ± 20° compared to the deposition direction. Although the HybHP yarn is more twisted than the H0 one (see Table 1 and Table 2), HybHP yarn is more easily oriented in the deposition direction, which can also explain the ease of the HybHP fibers to diffuse in the transverse direction from the U-turn. This enhanced mobility of the fibers with HybHP yarn to accept the strain applied by the deposition can originate from the lubrication-like effect of PLA on the fiber friction, as discussed previously.

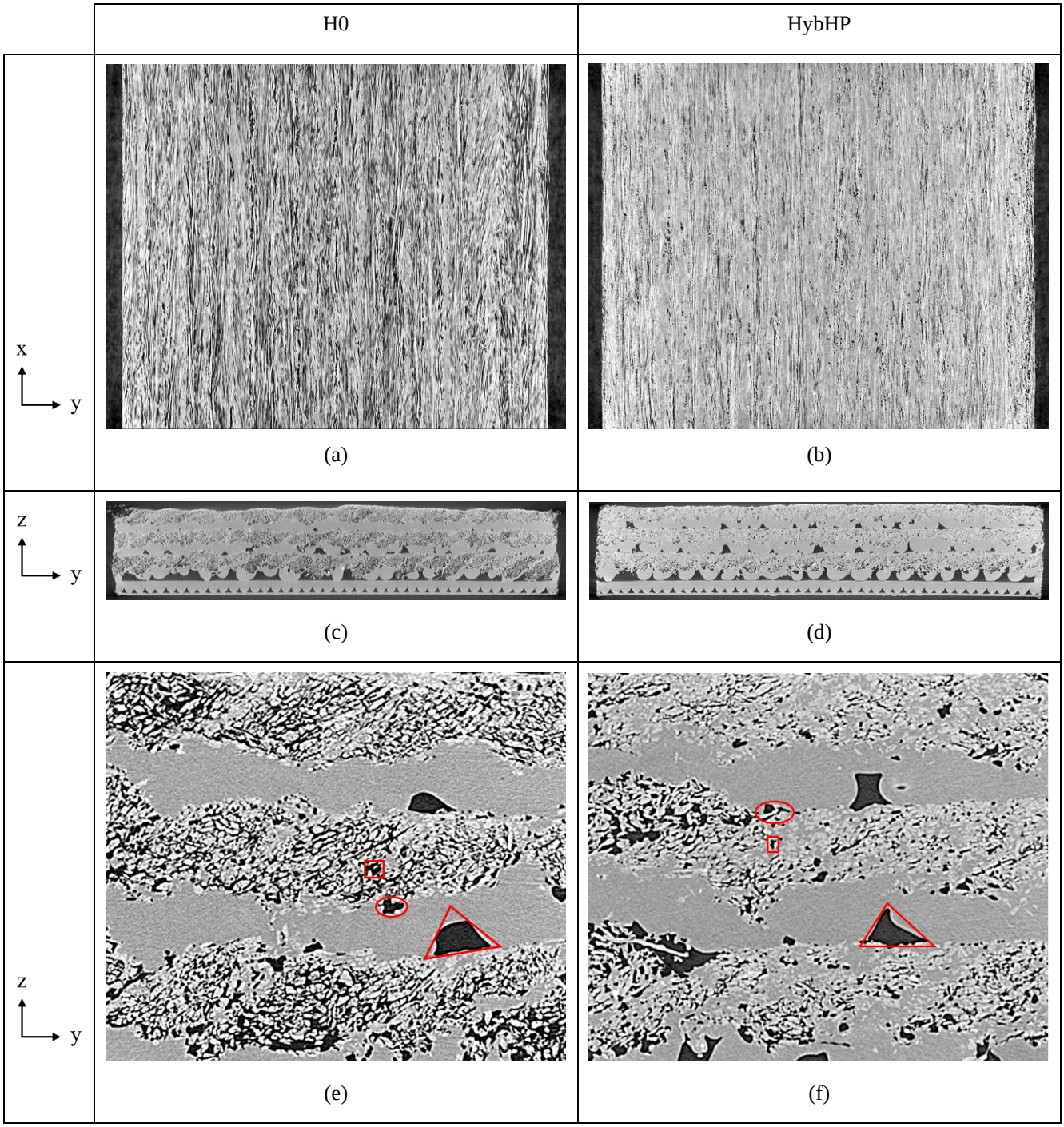

Figure 6. Tomographies in the gauge section of (a,c,e) H0 and (b,d,f) HybHP specimens, as seen (a,b) through an X-µCT cut in the plane of a HYRB layer, and (c,d,e,f) through an X-µCT, cut orthogonal to the deposition direction on (c,d) the whole cross-sectional area and (e,f) a zoomed area of the HYRB layers. Examples of the three kinds of voids are highlighted in (e,f) zoomed areas, namely inter-raster voids (in triangles), voids at the yarn/matrix interface (in ovals), and in-yarn voids (in rectangles).

Figure 6(c) and Figure 6(d) show examples of cross-sectional areas of H0 and HybHP specimens. This view is representative of the whole PLA and HYRB layers and their stacking sequence morphology. From bottom to top layers,

the inter-raster and inter-layer porosities are tighter and could come from a cumulative excess of materials due to too low layer height setting when the limit of compressibility of the twisted yarn is reached [37]. However, as seen in Figure 6(a) and Figure 6(b), both specimens present untwisted or low-twisted yarns and a tendency to accept the compression with a transverse diffusion of the fiber. A measurement of the dimensions for both HYRB-based specimens indicates a thickness of around 2.8 to 3.0 mm instead of the designed 2.1 mm, which would rather suggest a compression of the springs below the build plate that damps the stress applied on the yarns by the nozzle. This damping is reduced with the succession of layers as more and more dimensional deviation is cumulated, which is similar to a decrease in layer height setting that justifies the increase of pressure applied on the latter layers and, therefore, the reduced void content [37]. Following this compression, the last PLA layer that was initially designed in the sequence (see Figure 2b) for both HYRB-based specimens cannot be deposited as the pressure in the molten polymer was inferior to the pressure exerted between the nozzle and the last HYRB layer due to the accumulation of excess material.

The cut in the plane orthogonal to the deposition direction allows the observation of the inner composite raster morphology. Because of the ironing effect, the pultruded yarns tend to be placed at the upper side of the raster [56], but the disposition of the fibers is rather slantwise than horizontal for both HYRB-based specimens (see Figure 6(c) and Figure 6(d)). This gradual shift of the fibers in the transverse direction (y-axis) with the height (z-axis) arises from the neighboring deposition that causes a transverse displacement at the upper side of the previously deposited raster. Another explanation is that the over-pressure leads the raster to flow outside of its trajectory up to the lower side of the subsequent raster trajectory, which in turn would lead the next raster to be deposited on the upper side of its own trajectory and to flow the excess on the lower side of the next one. Whatever the case, this phenomenon can accentuate the transverse diffusion of the fibers and homogenize the distribution of the fibers in a same layer, exerting additional displacement that can locally untwist the yarns or at least disperse the fibers to facilitate the impregnation compared to highly twisted yarns [33,39].

A zoom on the in-plane cut orthogonal to the deposition direction gives a more precise view of the hemp/PLA/void architecture and more details on the hemp/PLA interface (see Figure 6(e) and Figure 6(f)). For both HYRB-based specimens, voids are in three different locations with specific morphologies. The first voids are large hypotrochoid-like porosities of the same magnitude order as the raster size and are located between these rasters. Those voids are already well-known in the literature. Previous studies detailed their irregularities and their formation with the printing strategy and evaluated their mechanical impact [49,59]. The second voids are medium-sized voids surrounding the yarns at the yarn/matrix interface. Those porosities ranging from 50 µm to 125 µm in width are contingent on the coating defect of the yarn by the molten polymer. Their occurrence can derive from a lack of pressure during coating [38], an air transfer from the yarn towards its surface after coating, or a displacement differential between fibers and matrix [60] during the

successive depositions with the transverse diffusion that causes hemp/PLA debonding. Those voids are few and equally observed in both HYRB-based specimens, showing a good coating quality for both specimens. The third voids are related to the impregnation quality, the lack of which forms air gaps between the hemp fibers. Unlike the previous yarn/matrix interfacial porosities, in-yarn porosities are not of the same content between H0 and HybHP specimens. H0 specimens show poor impregnation of the fibers with the presence of voids between most of the individual fibers (see Figure 6(e)). In contrast, fewer and smaller in-yarn voids are observed with HybHP specimens (see Figure 6(f)), meaning an improved impregnation rate with HybHP specimens compared to H0 ones. A reduction of these latter voids for the HybHP specimens lets predict a better stress transfer from the PLA matrix to the hemp fibers with a more developed fiber/matrix interface thanks to a greater impregnation rate. However, the range of gray levels on tomographies is sufficiently large to distinguish voids from matter, namely fiber and matrix, but not enough to segregate the elementary fibers from the matrix. This implies that comparison of the formulation composition between the two HYRB materials requires extraction of the fibers from the matrix to fully assess the composition with the aim of better predicting the mechanical properties.

3.2. Composition

Porosity rates were obtained from X-μCT analyses for both HYRB-based specimens, and solvent extraction was performed to determine fiber mass contents. The extracted fibers were supple again, and the absence of PLA residue was checked on digital 3D microscopy. Table 5 summarizes those results according to the different sampling zones as described in Figure 3. It appears the fiber mass fraction is lower for HybHP specimens compared to H0 ones, regardless of the contents in the HYRB layers than in the whole specimen, which is consistent with the addition of PLA fibers in the commingling process of hemp fibers that acted as a primary dilution of the hemp content in the yarns. On the opposite, this decrease in fiber content is accompanied by a drastic decrease in porosity rate inside the yarns by a factor of around 3 from H0 to HybHP specimens. To a lesser extent, the porosity rate is decreased by a factor of around 2 from H0 to HybHP specimens. This results in a different distribution of the kind of voids between the two HYRB-based specimens, where porosities are rather located inside the yarns for H0 specimens and quite well-balanced between inter-raster voids and inter-fiber voids for HybHP specimens. This porosity distribution imbalance and impoverishment in PLA around the hemp fibers for H0 specimens are expected to be detrimental to the mechanical reinforcement of the HYRB-based materials regarding low stress transfer and premature crack initiation due to local stress concentration.

Table 5. Summary of H0 and HybHP composition in fiber and void contents, with associated standard deviations, as determined by extraction and X-µCT methods in different sampling zones.

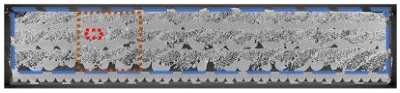
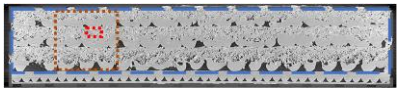

		H0	HybHP
Global fiber mass fraction		38.3 ± 0.4%	27.9 ± 0.1%
In-HYRB fiber mass fraction		47.7 ± 0.8%	33.3 ± 0.1%
In-HYRB porosity rate		25.7 ± 0.4%	14.1 ± 0.1%
In-yarn porosity rate		36.2 ± 0.3%	13.0 ± 0.3%

The compositions determined in Table 5 are expressed in volume for porosity rates and in mass for fiber contents. When studying composite materials, the ratio of the fibers is usually expressed in volume, in apparent or effective fractions. In addition, as porosity rates can range from single to double, the comparison of the fiber part in the HYRB layers between the two HYRB-based specimens is harsh to assess in mass when considering the global architecture that includes massless voids. Converting mass fractions into volume fractions is then required. Using void volume fractions and fiber mass fractions in Table 5, with PLA density being 1.24 g/cm^3 (see Table 3) and elementary hemp fiber density being 1.393 g/cm^3 [61], volume fractions in hemp fibers, in PLA, and in void are determined using equations (7) and (8) (see Supplementary data). The compositions in volume of HYRB layers for both HYRB-based specimens are reported in Table 6.

Table 6. Volume fractions in hemp fibers, in PLA matrix, and in void for H0 and HybHP specimens in the HYRB layers as determined by calculation from densities, extraction, and X-µCT methods.

	H0	HybHP
Hemp volume fraction	33.3%	26.4%
PLA volume fraction	41.0%	59.5%
Void volume fraction	25.7%	14.1%

Due to the higher void content in H0 specimens, the relative difference in hemp fraction between H0 and HybHP specimens is 21% in volume (see Table 6), while it was 30% in mass (see Table 5). One should note that HYRB layers in both specimens are preceded by PLA layers in their manufacturing that count for 25% of the volume of the whole specimen and would then dilute the hemp volume fraction and their reinforcement action during mechanical testing. From the literature [10,20], most of the continuous-reinforced composites by AM stand below 30% in fiber volume fraction in the YRC layers, which indicates that hemp volume fraction in HYRB layers of HypHP specimens stands at the upper limit and, for H0 specimens, just above this limit. Since lower hemp volume fraction and lower void volume fraction tend to be respectively

detrimental and beneficial regarding the mechanical properties, an antagonistic effect is expected when using HybHP yarns compared to H0 ones.

3.3. Mechanical properties

Tensile properties are analyzed based on the comparison of stress-strain curves for both HYRB-based specimens regarding Young's modulus, ultimate tensile strength (UTS), and elongation at break. Representative stress-strain curves are displayed in Figure 7 and depict the tensile behavior of H0 and HybHP specimens.

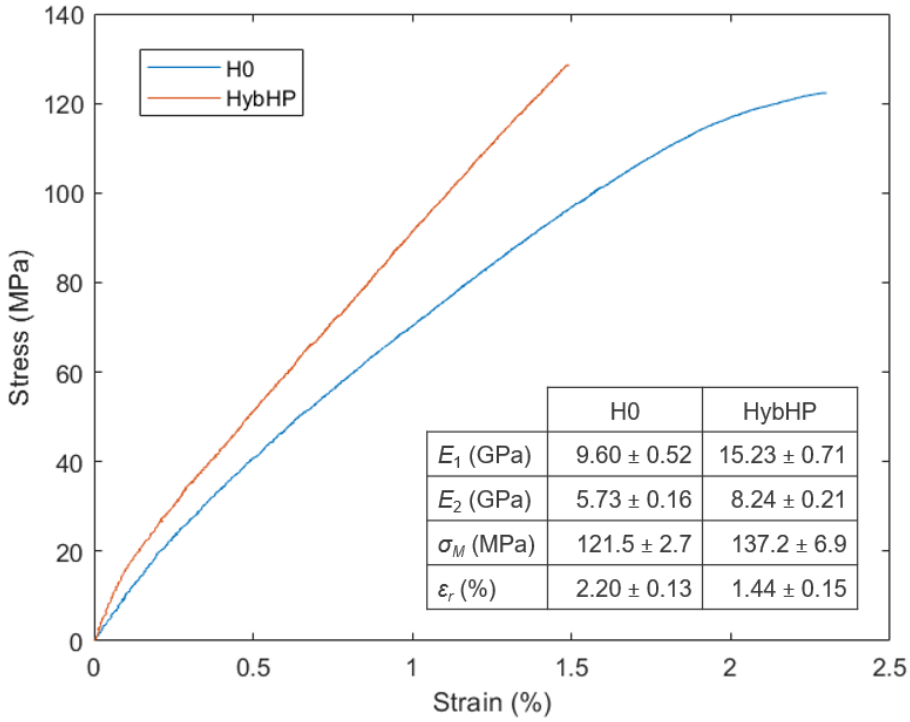

	H0	HybHP
E_1 (GPa)	9.60 ± 0.52	15.23 ± 0.71
E_2 (GPa)	5.73 ± 0.16	8.24 ± 0.21
σ_M (MPa)	121.5 ± 2.7	137.2 ± 6.9
ε_r (%)	2.20 ± 0.13	1.44 ± 0.15

Figure 7. Representative tensile stress-strain curves for H0 and HybHP specimens, and corresponding mean values of Young's modulus in the first stage (E_1), Young's modulus in the second stage (E_2), ultimate tensile strength (σ_M), and elongation at break (ε_r), with associated standard deviations.

Both specimens consist of a first linear stage rapidly followed by a transitional non-linear stage and a second linear one. The end of the first stage is called the yield stress and is reached around 18 MPa for both specimens. This yield occurs around 0.1% in strain for HybHP specimens and 0.2% for H0 specimens, where stiffness suffers from a 46% loss in Young's modulus for HybHP and 40% for H0 specimens once in the second linear stage, which is consistent with the mechanical behavior of YRC in the literature [62].

Despite its lower fiber volume fraction (see Table 6), HybHP specimens show higher mechanical properties than the H0 ones with an increase of 59% on the first modulus, 44% on the second modulus, and 13% on the UTS (see Figure 7). This can be explained by the more developed hemp fiber/PLA interface for the HybHP biocomposite that allows more efficient stress transfer from the matrix to the fibers, as well as by an increased fibers alignment in the tensile direction, leading all the fibers to contribute to the mechanical behavior. Indeed, it has been shown (see 3.1. section) that HybHP fibers are mostly aligned in the deposition direction, i.e. unidirectionally oriented at 0° while those of H0 material are oriented at various angles from 0° up to ± 20° (see Figure 6(a) and Figure 6(b)). However, the composition is not the same between the two materials (see Table 6) and a decrease in fiber volume fraction and void volume fraction when using HybHP yarns would cause both a decrease and an increase in the mechanical properties. To consider the mechanical properties without the voids, the use of a scaling coefficient $K = 1/(1 - \Phi_{v,V})$ can return an effective Young's modulus such as the effective Young's modulus in the first stage is 17.73 GPa for HybHP specimens and 12.92 GPa for H0 ones. This means that the use of HybHP still allows an increase of 37% in stiffness while the fiber volume fraction is 21% lower, showing the interest in first ensuring a good impregnation and alignment of the fibers before increasing their volume fraction in the composite. The stiffness of HybHP specimens is then close to the stiffness of elementary hemp fiber, which is between 13 to 23 GPa, and around 19.1 GPa at a similar 50% humidity rate (see 2.3. Characterization and extraction) [63].

Data in the literature indicate mechanical properties well below those of HybHP specimens when comparing additively manufactured composites filled with 5 to 10% in short hemp fibers whose Young's modulus and UTS were respectively around 0.9 to 2.8 GPa and 28 to 37 MPa [64–66]. With YRC obtained by continuous AM, Young's modulus ranges from 5 to 23 GPa and UTS from 50 to 250 MPa [20]. This locates the HybHP mechanical properties just below the highest obtained properties with flax fibers [33], knowing that removing the adhesion PLA layer that takes 25% of the specimen could even get the mechanical properties closer to this upper limit. If considering similar hybrid hemp fibers but with conventional composites, mechanical properties of HybHP specimens are superior as Young's modulus and UTS can respectively reach 1.2 GPa and 64 MPa with hemp/PA11 hybrid yarns-based bidirectional composites at 52% in fiber mass fraction [67] and 6.6 GPa and 59 MPa with hemp/PLA hybrid yarns-based bidirectional composites at 45% in fiber mass fraction [68]. HybHP mechanical properties are even similar to those from unidirectional composites based on long hemp fibers and epoxy thermoset polymer that reach 10.5 GPa in Young's modulus and 167 MPa in UTS with 32% in mass fraction [69] or 12.7 GPa and 106 MPa at 30% in volume fraction [70]. One should note that Lu et al. [69] attained 16% in void volume fraction with epoxy resin, which is similar to the 14% in HybHP specimens (see Table 6), even though PLA thermoplastic polymer is more viscous and would make it difficult to perform impregnation compared to epoxy resin.

A closer look at the transitional non-linear stage reveals differences between H0 and HybHP specimens (see Figure 7). On one hand, H0's non-linear stage starts at 0.2% in strain and continues up to 0.6% in a staggered and mild transition. On the other hand, HybHP's non-linear stage shows a clear and prompt transition at 0.1%. This non-linear stage is not fully understood since it originates from several phenomena, mainly due to fiber/matrix debonding and fiber/fiber unbundling, and partially due to the non-linear behavior of the elementary fibers, namely re-orientation of cellulose micro-fibrils and crystallization of their amorphous phase [33,62,71,72]. In the case of H0 specimens, the lack of impregnation leaves a fiber/matrix interface limited to the surrounding of the yarns, through the coating interface, for the benefit of fiber/fiber interactions inside the yarns. This implies a gradient of stress transfer from the matrix to the surrounding fibers and then to the fibers inside, whose debonding at the non-linear stage happens on an extensive range of strain due to a stick-slip mechanism from fiber/fiber interactions [62]. On the contrary, HybHP specimens are mostly subjected to matrix/fiber interactions due to the high impregnation rate, whose debonding occurs sharply with little stick-slip mechanism because of fewer fiber/fiber interactions compared to H0 specimens. These different observations are in agreement with the literature where the larger range of strain in H0's non-linear stage is representative of additively manufactured YRC [33,71]. In contrast, a sharper transition was mainly observed with conventional composites whose impregnation was achieved like in HybHP specimens [70].

Following the second linear stage, H0 and HybHP specimens undergo different mechanical behaviors about damage mechanisms (see Figure 7). While HybHP specimens show brittle behavior with abrupt rupture at the end of the linear stage at 1.4% in strain, H0 specimens present a quasi-ductile behavior with a plastic deformation from the end of the linear stage at 1.4% to the rupture at 2.2% in strain. This limit of 1.4% in strain, where the mechanical behaviors differ between the two HYRB-based materials, corresponds to the failure of the PLA matrix after which damage on yarns occurs with yarn unwinding, fiber/fiber sliding, fiber breakage, and fiber pull-out for H0 specimens (see Figure 8). This damage behavior is consistent with previous studies in the literature when twisted dried yarns are not impregnated, leading to weak fiber/matrix interactions [33,38]. On the other side, HybHP specimens endure a neater rupture with cracks propagating in the transverse direction that reflects a good adhesion between the PLA matrix and the hemp fibers as PLA cracking pursues through the hemp fibers without or with few fiber pull-outs and without sliding at fiber/fiber interface (see Figure 9).

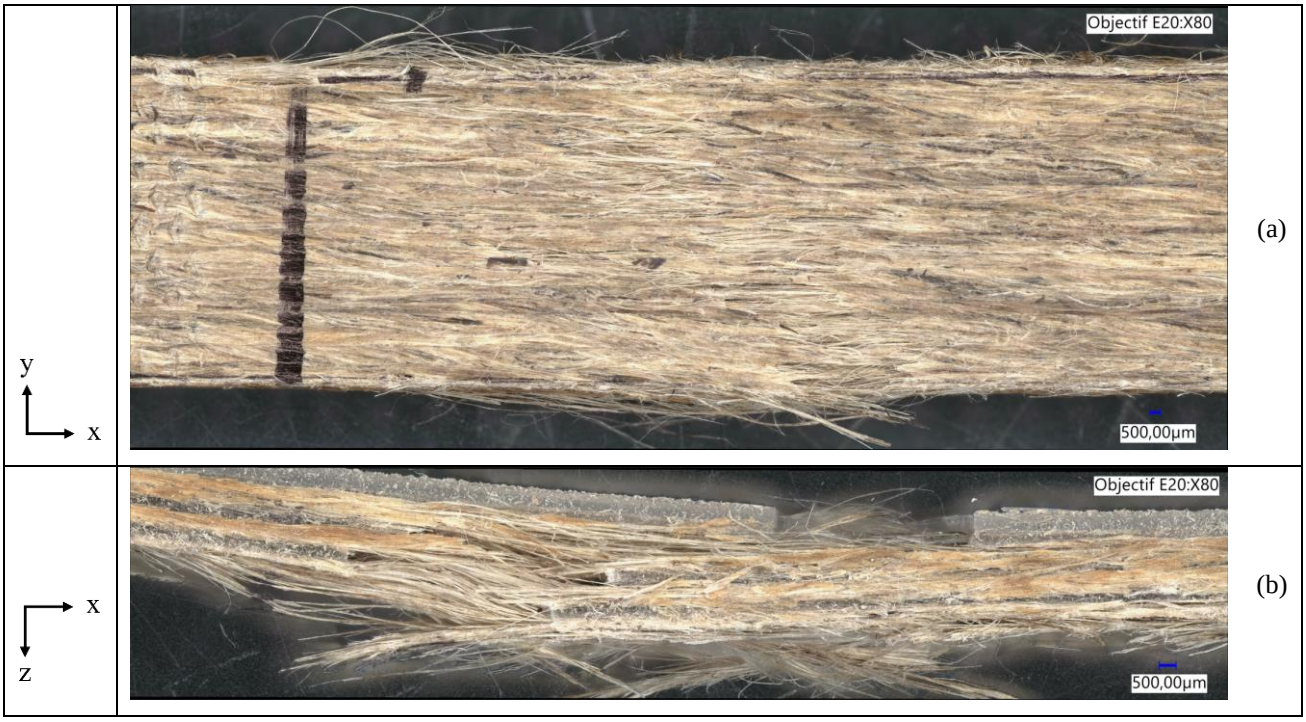

Figure 8. Digital 3D micrographies of H0 specimens after fracture as seen from (a) top view and (b) side view.

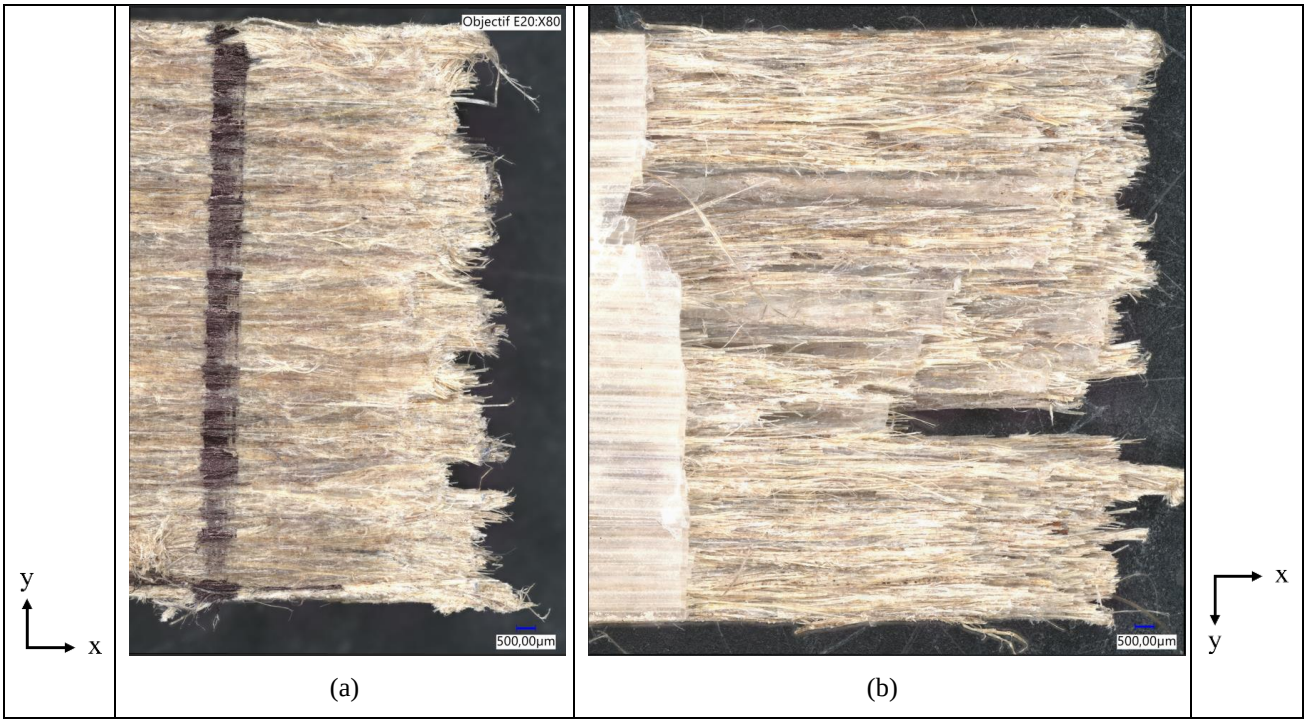

Figure 9. Digital 3D micrographies of HybHP specimens after fracture as seen from (a) top view and (b) bottom view.

4. Conclusions and perspectives

Hemp yarns were used for the first time in AM to produce HYRB materials. A new preparation method based on plant/polymer fibers commingling was proposed to improve the yarn impregnation after printing. The addition of PLA

fibers to the hemp fibers tended to dilute the hemp content in the end material formulation. Still, several advantages were observed thanks to the presence of PLA between the hemp fibers, namely reduced void content, more aligned fibers, more homogeneous distribution of the fibers, matrix, and voids, and better dimensional accuracy. Those differences in composition and morphology led to an increase in stress transfer from the matrix to the fibers with the use of hybrid yarns and then to a more brittle behavior with a stiffer and more resistant biocomposite compared to the one that was produced with pure hemp yarns. As a result, the decrease in hemp fiber content with the commingling was not detrimental to the quality and performance of the biocomposite materials; quite the contrary. Consequently, improving the impregnation of the yarns is of major importance and should be studied at the same level as the increase in fiber content. Although the nature and structure of the twisted plant-based yarns could lead to a lack of impregnation by the viscous molten thermoplastic, this improved impregnation method allowed the development of the mechanical performance to the level of that of conventionally manufactured composites based on plant-based reinforcements. One should note that this commingling/AM method can be transposed to other yarns based on plant fibers to produce and expand the range of available biocomposites, meeting high customization, high performance, and eco-design requirements.

In this study, pure hemp yarns were coextruded with a PLA filament, and so were hybrid yarns for comparison. This complementary addition of PLA and the tensile force applied on the yarn led to a certain inhomogeneity at the raster scale as the hemp fibers tend to be located at the upper side of the deposition, while a more dispersed morphology of the fibers would improve the stress transfer from the matrix to the reinforcements. Future studies should focus on the sole use of hybrid yarns without the complement use of a thermoplastic filament to increase the fiber content in the biocomposite and to improve the material's homogeneity. Improving the impregnation, the fiber content, and the fiber distribution is thought to be a new gap in the manufacturing of high-performance biocomposites by AM for the development of such technology for sustainable, lightweight, and high-end applications.

Acknowledgments

This project is included in the MATUR Chair, co-financed by the Grand Est Region (France) and the Ardenne Metropole. The authors gratefully acknowledge the Italian company Linificio and Canapificio Nazionale (LCN) for providing the hemp rovings used in the “European Union’s Horizon 2020” Research and Innovation Program with Grant Agreement No. 744349 – SSUCHY Project”. Platinium 3D (France) is also thanked for granting access to the digital 3D microscope and their technical assistance in the image acquisitions.

Appendix A. Supplementary data

Without considering the void in a first step, and knowing respectively the fiber mass fraction $\varphi_{m,F}$ and the fiber volume fraction $\varphi_{v,F}$ in function of the fiber mass m_F, polymer mass m_P, fiber volume V_F and polymer volume V_P, equations (1) and (2) read:

$$\varphi_{m,F} = \frac{m_F}{m_F + m_P} \tag{1}$$

$$\varphi_{v,F} = \frac{V_F}{V_F + V_P} \tag{2}$$

The ratio of fiber fractions can then be expressed as:

$$\frac{\varphi_{m,F}}{\varphi_{v,F}} = \frac{m_F}{V_F} \times \frac{V_F + V_P}{m_F + m_P} \tag{3}$$

Knowing the relation between the density ρ, the mass m, and the volume V as $\rho = m/V$, all volume terms can be replaced in equation (3) as:

$$\frac{\varphi_{m,F}}{\varphi_{v,F}} = \rho_F \times \frac{m_F/\rho_F + m_P/\rho_P}{m_F + m_P} \tag{4}$$

With ρ_F the density of the elementary fiber and ρ_P the density of the polymer. By using equation (1) and knowing that everything that is not fiber is polymer in mass such as polymer mass fraction is $\varphi_{m,P} = \frac{m_P}{m_F+m_P} = 1 - \varphi_{m,F}$, all mass terms can be replaced, and equation (4) can be written as:

$$\frac{\varphi_{m,F}}{\varphi_{v,F}} = \rho_F \times \left[\frac{\varphi_{m,F}}{\rho_F} + \frac{(1 - \varphi_{m,F})}{\rho_P}\right] \tag{5}$$

Fiber volume fraction is then expressed with the densities and the fiber mass fraction as:

$$\varphi_{v,F} = \frac{\rho_P}{\rho_P + \rho_F/\varphi_{m,F} - \rho_F} \tag{6}$$

When considering in the second step the voids in the fiber/polymer/void system, with void volume fraction $\Phi_{v,V}$ being determined by X-µCT analyses, fiber volume fraction in HYRB layers $\Phi_{v,F}$ is established as:

$$\Phi_{v,F} = \frac{\rho_P \times (1 - \Phi_{v,V})}{\rho_P + \rho_F/\varphi_{m,F} - \rho_F} \tag{7}$$

And everything that is not fiber or void in this fiber/polymer/void system is polymer, such as polymer volume fraction in HYRB layers is:

$$\Phi_{v,P} = 1 - \Phi_{v,F} - \Phi_{v,V} \tag{8}$$

References

[1] Guo N, Leu MC. Additive manufacturing: technology, applications, and research needs. Front Mech Eng 2013;8:215–43. https://doi.org/10.1007/s11465-013-0248-8.

[2] Tofail SAM, Koumoulos EP, Bandyopadhyay A, Bose S, O'Donoghue L, Charitidis C. Additive manufacturing: scientific and technological challenges, market uptake and opportunities. Mater Today 2018;21:22–37. https://doi.org/10.1016/j.mattod.2017.07.001.

[3] Matsuzaki R, Ueda M, Namiki M, Jeong T-K, Asahara H, Horiguchi K, et al. Three-dimensional printing of continuous-fiber composites by in-nozzle impregnation. Sci Rep 2016;6:23058. https://doi.org/10.1038/srep23058.

[4] Srivastava M, Rathee S, Patel V, Kumar A, Koppad PG. A review of various materials for additive manufacturing: Recent trends and processing issues. J Mater Res Technol 2022;21:2612–41. https://doi.org/10.1016/j.jmrt.2022.10.015.

[5] Liu G, Xiong Y, Zhou L. Additive manufacturing of continuous fiber reinforced polymer composites: Design opportunities and novel applications. Compos Commun 2021;27:100907. https://doi.org/10.1016/j.coco.2021.100907.

[6] Bekas DG, Hou Y, Liu Y, Panesar A. 3D printing to enable multifunctionality in polymer-based composites: A review. Compos Part B Eng 2019;179:107540. https://doi.org/10.1016/j.compositesb.2019.107540.

[7] Ginoux G, Dony P, Vroman I, Alix S. Improving thermomechanical properties of fused filament fabrication printed parts by using nanocomposites. Compos Part B Eng 2021;224:109227. https://doi.org/10.1016/j.compositesb.2021.109227.

[8] Wang X, Jiang M, Zhou Z, Gou J, Hui D. 3D printing of polymer matrix composites: A review and prospective. Compos Part B Eng 2017;110:442–58. https://doi.org/10.1016/j.compositesb.2016.11.034.

[9] Zhuo P, Li S, Ashcroft IA, Jones AI. Material extrusion additive manufacturing of continuous fibre reinforced polymer matrix composites: A review and outlook. Compos Part B Eng 2021;224:109143. https://doi.org/10.1016/j.compositesb.2021.109143.

[10] Cheng P, Peng Y, Li S, Rao Y, Le Duigou A, Wang K, et al. 3D printed continuous fiber reinforced composite lightweight structures: A review and outlook. Compos Part B Eng 2023;250:110450. https://doi.org/10.1016/j.compositesb.2022.110450.

[11] Cheng P, Li S, Peng Y, Duigou AL, Wang K, Ahzi S. 3D/4D Printed Functional Continuous Fiber-reinforced Polymer Composites: Progress and Perspectives. Chin J Mech Eng Addit Manuf Front 2023;2:100090. https://doi.org/10.1016/j.cjmeam.2023.100090.

[12] Safari F, Kami A, Abedini V. 3D printing of continuous fiber reinforced composites: A review of the processing, pre- and post-processing effects on mechanical properties. Polym Polym Compos 2022;30:096739112210987. https://doi.org/10.1177/09673911221098734.

[13] Kasmi S, Ginoux G, Allaoui S, Alix S. Investigation of 3D printing strategy on the mechanical performance of coextruded continuous carbon fiber reinforced PETG. J Appl Polym Sci 2021;138:50955. https://doi.org/10.1002/app.50955.

[14] Yu S, Hwang YH, Hwang JY, Hong SH. Analytical study on the 3D-printed structure and mechanical properties of basalt fiber-reinforced PLA composites using X-ray microscopy. Compos Sci Technol 2019;175:18–27. https://doi.org/10.1016/j.compscitech.2019.03.005.

[15] Balla VK, Kate KH, Satyavolu J, Singh P, Tadimeti JGD. Additive manufacturing of natural fiber reinforced polymer composites: Processing and prospects. Compos Part B Eng 2019;174:106956. https://doi.org/10.1016/j.compositesb.2019.106956.

[16] Muthe LP, Pickering K, Gauss C. A Review of 3D/4D Printing of Poly-Lactic Acid Composites with Bio-Derived Reinforcements. Compos Part C Open Access 2022;8:100271. https://doi.org/10.1016/j.jcomc.2022.100271.

[17] Liu T, Butaud P, Placet V, Ouisse M. Damping behavior of plant fiber composites: A review. Compos Struct 2021;275:114392. https://doi.org/10.1016/j.compstruct.2021.114392.

[18] Zhang Z, Cai S, Li Y, Wang Z, Long Y, Yu T, et al. High performances of plant fiber reinforced composites—A new insight from hierarchical microstructures. Compos Sci Technol 2020;194:108151. https://doi.org/10.1016/j.compscitech.2020.108151.

[19] Li M, Pu Y, Thomas VM, Yoo CG, Ozcan S, Deng Y, et al. Recent advancements of plant-based natural fiber–reinforced composites and their applications. Compos Part B Eng 2020;200:108254. https://doi.org/10.1016/j.compositesb.2020.108254.

[20] Tao Y, Li P, Zhang J, Wang S, Shi SQ, Kong F. A review of fused filament fabrication of continuous natural fiber reinforced thermoplastic composites: Techniques and materials. Polym Compos 2023:pc.27477. https://doi.org/10.1002/pc.27477.

[21] Santos NV, Cardoso DCT. 3D printing of vegetable yarn-reinforced polymer components. J Clean Prod 2023;415:137870. https://doi.org/10.1016/j.jclepro.2023.137870.

[22] Ahmed ATMF, Islam MZ, Mahmud MS, Sarker ME, Islam MR. Hemp as a potential raw material toward a sustainable world: A review. Heliyon 2022;8:e08753. https://doi.org/10.1016/j.heliyon.2022.e08753.

[23] Le Duigou A, Correa D, Ueda M, Matsuzaki R, Castro M. A review of 3D and 4D printing of natural fibre biocomposites. Mater Des 2020;194:108911. https://doi.org/10.1016/j.matdes.2020.108911.

[24] Van Der Werf HMG, Turunen L. The environmental impacts of the production of hemp and flax textile yarn. Ind Crops Prod 2008;27:1–10. https://doi.org/10.1016/j.indcrop.2007.05.003.

[25] Amaducci S, Scordia D, Liu FH, Zhang Q, Guo H, Testa G, et al. Key cultivation techniques for hemp in Europe and China. Ind Crops Prod 2015;68:2–16. https://doi.org/10.1016/j.indcrop.2014.06.041.

[26] Pervaiz M, Sain MM. Carbon storage potential in natural fiber composites. Resour Conserv Recycl 2003;39:325–40. https://doi.org/10.1016/S0921-3449(02)00173-8.

[27] Angelova V, Ivanova R, Delibaltova V, Ivanov K. Bio-accumulation and distribution of heavy metals in fibre crops (flax, cotton and hemp). Ind Crops Prod 2004;19:197–205. https://doi.org/10.1016/j.indcrop.2003.10.001.

[28] Aryal K, Maraseni T, Kretzschmar T, Chang D, Naebe M, Neary L, et al. Knowledge mapping for a secure and sustainable hemp industry: A systematic literature review. Case Stud Chem Environ Eng 2024;9:100550. https://doi.org/10.1016/j.cscee.2023.100550.

[29] Marrot L, Lefeuvre A, Pontoire B, Bourmaud A, Baley C. Analysis of the hemp fiber mechanical properties and their scattering (Fedora 17). Ind Crops Prod 2013;51:317–27. https://doi.org/10.1016/j.indcrop.2013.09.026.

[30] Beaugrand J, Guessasma S, Maigret J-E. Damage mechanisms in defected natural fibers. Sci Rep 2017;7:14041. https://doi.org/10.1038/s41598-017-14514-6.

[31] Placet V, François C, Day A, Beaugrand J, Ouagne P. Industrial Hemp Transformation for Composite Applications: Influence of Processing Parameters on the Fibre Properties. In: Fangueiro R, Rana S, editors. Adv. Nat. Fibre Compos., Cham: Springer International Publishing; 2018, p. 13–25. https://doi.org/10.1007/978-3-319-64641-1_2.

[32] Gabrion X, Koolen G, Grégoire M, Musio S, Bar M, Botturi D, et al. Influence of industrial processing parameters on the effective properties of long aligned European hemp fibres in composite materials. Compos Part Appl Sci Manuf 2022;157:106915. https://doi.org/10.1016/j.compositesa.2022.106915.

[33] Le Duigou A, Barbé A, Guillou E, Castro M. 3D printing of continuous flax fibre reinforced biocomposites for structural applications. Mater Des 2019;180:107884. https://doi.org/10.1016/j.matdes.2019.107884.

[34] Terekhina S, Egorov S, Tarasova T, Skornyakov I, Guillaumat L, Hattali ML. In-nozzle impregnation of continuous textile flax fiber/polyamide 6 composite during FFF process. Compos Part Appl Sci Manuf 2022;153:106725. https://doi.org/10.1016/j.compositesa.2021.106725.

[35] Kabir SMF, Mathur K, Seyam A-FM. A critical review on 3D printed continuous fiber-reinforced composites: History, mechanism, materials and properties. Compos Struct 2020;232:111476. https://doi.org/10.1016/j.compstruct.2019.111476.

[36] Kabir MM, Wang H, Lau KT, Cardona F. Chemical treatments on plant-based natural fibre reinforced polymer composites: An overview. Compos Part B Eng 2012;43:2883–92. https://doi.org/10.1016/j.compositesb.2012.04.053.

[37] Le Duigou A, Chabaud G, Matsuzaki R, Castro M. Tailoring the mechanical properties of 3D-printed continuous flax/PLA biocomposites by controlling the slicing parameters. Compos Part B Eng 2020;203:108474. https://doi.org/10.1016/j.compositesb.2020.108474.

[38] Cheng P, Wang K, Chen X, Wang J, Peng Y, Ahzi S, et al. Interfacial and mechanical properties of continuous ramie fiber reinforced biocomposites fabricated by in-situ impregnated 3D printing. Ind Crops Prod 2021;170:113760. https://doi.org/10.1016/j.indcrop.2021.113760.

[39] Yang Z, Zhang Z, Long Y, Fu K, Li Y. Process optimization of continuous flax fiber/polylactic acid prepreg filaments toward high performance 3D -printed composites. Polym Compos 2023;44:6242–53. https://doi.org/10.1002/pc.27559.

[40] Wu X, Ginoux G, Allaoui S. Formulation of bio-based composite filaments by extrusion/coating for fused filament fabrication: a structural and mechanical analysis 2021.

[41] Vaneker THJ. Material Extrusion of Continuous Fiber Reinforced Plastics Using Commingled Yarn. Procedia CIRP 2017;66:317–22. https://doi.org/10.1016/j.procir.2017.03.367.

[42] Zhuo P, Li S, Ashcroft IA, Jones IA. Continuous fibre composite 3D printing with pultruded carbon/PA6 commingled fibres: Processing and mechanical properties. Compos Sci Technol 2022;221:109341. https://doi.org/10.1016/j.compscitech.2022.109341.

[43] Alagirusamy R, Fangueiro R, Ogale V, Padaki N. Hybrid Yarns and Textile Preforming for Thermoplastic Composites. Text Prog 2006;38:1–71. https://doi.org/10.1533/tepr.2006.0004.

[44] Laqraa C, Labanieh AR, Soulat D, Ferreira M. Development of woven and quasi-unidirectional reinforcement fabrics with hemp fibers: study of mechanical and preforming behaviors. Int J Mater Form 2022;16:8. https://doi.org/10.1007/s12289-022-01727-y.

[45] Corbin A-C, Soulat D, Ferreira M, Labanieh A-R. Influence of Process Parameters on Properties of Hemp Woven Reinforcements for Composite Applications: Mechanical Properties, Bias-extension Tests and Fabric Forming. J Nat Fibers 2022;19:714–26. https://doi.org/10.1080/15440478.2020.1761925.

[46] Corbin A-C, Soulat D, Ferreira M, Labanieh A-R, Gabrion X, Malécot P, et al. Towards hemp fabrics for high-performance composites: Influence of weave pattern and features. Compos Part B Eng 2020;181:107582. https://doi.org/10.1016/j.compositesb.2019.107582.

[47] Laqraa C, Ferreira M, Rashed Labanieh A, Soulat D. Elaboration by Wrapping Process and Multiscale Characterisation of Thermoplastic Bio-Composite Based on Hemp/PA11 Constituents. Coatings 2021;11:770. https://doi.org/10.3390/coatings11070770.

[48] Corbin A-C, Ferreira M, Labanieh AR, Soulat D. Natural fiber composite manufacture using wrapped hemp roving with PA12. Mater Today Proc 2020;31:S329–34. https://doi.org/10.1016/j.matpr.2020.02.307.

[49] Ginoux G, Paux J, Allaoui S. New preparation method of microstructurally and mechanically standardized PETG specimens by material extrusion additive manufacturing and machining. Addit Manuf 2023;66:103471. https://doi.org/10.1016/j.addma.2023.103471.

[50] Wang Q, Ji C, Sun J, Zhu Q, Liu J. Structure and Properties of Polylactic Acid Biocomposite Films Reinforced with Cellulose Nanofibrils. Molecules 2020;25:3306. https://doi.org/10.3390/molecules25143306.

[51] Oza S, Ning H, Ferguson I, Lu N. Effect of surface treatment on thermal stability of the hemp-PLA composites: Correlation of activation energy with thermal degradation. Compos Part B Eng 2014;67:227–32. https://doi.org/10.1016/j.compositesb.2014.06.033.

[52] Long Y, Zhang Z, Fu K, Li Y. Efficient plant fibre yarn pre-treatment for 3D printed continuous flax fibre/poly(lactic) acid composites. Compos Part B Eng 2021;227:109389. https://doi.org/10.1016/j.compositesb.2021.109389.

[53] Fruleux T, Castro M, Sauleau P, Matsuzaki R, Le Duigou A. Matrix stiffness: A key parameter to control hydro-elasticity and morphing of 3D printed biocomposite. Compos Part Appl Sci Manuf 2022;156:106882. https://doi.org/10.1016/j.compositesa.2022.106882.

[54] Kajbič J, Fajdiga G, Klemenc J. Material extrusion 3D printing of biodegradable composites reinforced with continuous flax fibers. J Mater Res Technol 2023;27:3610–20. https://doi.org/10.1016/j.jmrt.2023.10.148.

[55] De Kergariou C, Saidani-Scott H, Perriman A, Scarpa F, Le Duigou A. The influence of the humidity on the mechanical properties of 3D printed continuous flax fibre reinforced poly(lactic acid) composites. Compos Part Appl Sci Manuf 2022;155:106805. https://doi.org/10.1016/j.compositesa.2022.106805.

[56] Zhang Z, Long Y, Yang Z, Fu K, Li Y. An investigation into printing pressure of 3D printed continuous carbon fiber reinforced composites. Compos Part Appl Sci Manuf 2022;162:107162. https://doi.org/10.1016/j.compositesa.2022.107162.

[57] Liu S, Li Y, Li N. A novel free-hanging 3D printing method for continuous carbon fiber reinforced thermoplastic lattice truss core structures. Mater Des 2018;137:235–44. https://doi.org/10.1016/j.matdes.2017.10.007.

[58] Zhang P, Sun S, Duan J, Fu H, Han Z, Geng H, et al. Line width prediction and mechanical properties of 3D printed continuous fiber reinforced polypropylene composites. Addit Manuf 2023;61:103372. https://doi.org/10.1016/j.addma.2022.103372.

[59] Paux J, Ginoux G, Pulickan S, Allaoui S. Influence of printing irregularities on the elastic behavior and mesostructural stress concentrations in material extrusion additive manufacturing—A numerical approach based on X-ray tomography. Addit Manuf 2023;76:103760. https://doi.org/10.1016/j.addma.2023.103760.

[60] Tekinalp HL, Kunc V, Velez-Garcia GM, Duty CE, Love LJ, Naskar AK, et al. Highly oriented carbon fiber–polymer composites via additive manufacturing. Compos Sci Technol 2014;105:144–50. https://doi.org/10.1016/j.compscitech.2014.10.009.

[61] Rohen LA, Neves ACC, de P. Mantovani D, Carlos Maurício FV, da Silva Vieira J, de A. Pontes L, et al. Hemp Fiber Density Using the Pycnometry Technique. In: Ikhmayies S, Li B, Carpenter JS, Li Ji, Hwang J-Y, Monteiro SN, et al., editors. Charact. Miner. Met. Mater. 2017, Cham: Springer International Publishing; 2017, p. 423–8. https://doi.org/10.1007/978-3-319-51382-9_46.

[62] Shah DU. Damage in biocomposites: Stiffness evolution of aligned plant fibre composites during monotonic and cyclic fatigue loading. Compos Part Appl Sci Manuf 2016;83:160–8. https://doi.org/10.1016/j.compositesa.2015.09.008.

[63] Placet V, Cisse O, Boubakar ML. Influence of environmental relative humidity on the tensile and rotational behaviour of hemp fibres. J Mater Sci 2012;47:3435–46. https://doi.org/10.1007/s10853-011-6191-3.

[64] Dönitz A, Köllner A, Richter T, Löschke O, Auhl D, Völlmecke C. Additive Manufacturing of Biodegradable Hemp-Reinforced Polybutylene Succinate (PBS) and Its Mechanical Characterization. Polymers 2023;15:2271. https://doi.org/10.3390/polym15102271.

[65] Doğru A, Sözen A, SeydiBeyoğlu MÖ, Neşer G. Hemp Reinforced Polylactic Acid (PLA) Composite Produced By Fused Filament Fabrication (FFF). Hacet J Biol Chem 2022;50:239–46. https://doi.org/10.15671/hjbc.1032298.

[66] Arnold J, Smith DA. 3D printed polylactic acid - hemp fiber composites: Mechanical, thermal, and microcomputed tomography data. Data Brief 2021;39:107534. https://doi.org/10.1016/j.dib.2021.107534.

[67] Laqraa C, Ferreira M, Soulat D, Labanieh A-R. Natural Fibre Composites Manufacture using Wrapped Hemp Roving with PA11. Mater Circ Econ 2022;4:17. https://doi.org/10.1007/s42824-022-00057-3.

[68] Baghaei B, Skrifvars M, Berglin L. Manufacture and characterisation of thermoplastic composites made from PLA/hemp co-wrapped hybrid yarn prepregs. Compos Part Appl Sci Manuf 2013;50:93–101. https://doi.org/10.1016/j.compositesa.2013.03.012.

[69] Lu C, Wang C, Liu S, Zhang H, Tong J, Yi X, et al. Towards high-performance textile-structure composite: Unidirectional hemp fiber tape and their composite. Ind Crops Prod 2022;189:115821. https://doi.org/10.1016/j.indcrop.2022.115821.

[70] Lebrun G, Couture A, Laperrière L. Tensile and impregnation behavior of unidirectional hemp/paper/epoxy and flax/paper/epoxy composites. Compos Struct 2013;103:151–60. https://doi.org/10.1016/j.compstruct.2013.04.028.

[71] Monti A, El Mahi A, Jendli Z, Guillaumat L. Mechanical behaviour and damage mechanisms analysis of a flax-fibre reinforced composite by acoustic emission. Compos Part Appl Sci Manuf 2016;90:100–10. https://doi.org/10.1016/j.compositesa.2016.07.002.

[72] Placet V, Cissé O, Lamine Boubakar M. Nonlinear tensile behaviour of elementary hemp fibres. Part I: Investigation of the possible origins using repeated progressive loading with in situ microscopic observations. Compos Part Appl Sci Manuf 2014;56:319–27. https://doi.org/10.1016/j.compositesa.2012.11.019.